Insights on the Surge Behavior of Storstrømmen and L. Bistrup Bræ, Northeast Greenland, Over the Last Century

J. Mouginot, A. Bjørk, R. Millan, B. Scheuchl, E. Rignot

AGU100 ADVANCING EARTH AND SPACE SCIENCE

Geophysical Research Letters

RESEARCH LETTER
10.1029/2018GL079052

Key Points:
- A multisensor approach combining historical with modern remote sensing data sets is used to document the history of the largest surging glaciers in the world
- We are able to analyze and interpret pattern of retreat, speedup, and thinning over the last century
- A surge cycle is accurately estimated and we forecast the next surge under current climatic conditions

Supporting Information:
- Supporting Information S1

Correspondence to:
J. Mouginot,
jmougino@uci.edu

Citation:
Mouginot, J., Bjørk, A. A., Millan, R., Scheuchl, B., & Rignot, E. (2018). Insights on the surge behavior of Storstrømmen and L. Bistrup Bræ, northeast Greenland, over the last century. *Geophysical Research Letters*, *45*, 11,197–11,205. https://doi.org/10.1029/2018GL079052

Received 5 JUN 2018
Accepted 29 SEP 2018
Accepted article online 4 OCT 2018
Published online 23 OCT 2018

Insights on the Surge Behavior of Storstrømmen and L. Bistrup Bræ, Northeast Greenland, Over the Last Century

J. Mouginot[1,2], A. A. Bjørk[1,3], R. Millan[1,2], B. Scheuchl[1], and E. Rignot[1,4]

[1]Department of Earth System Science, University of California, Irvine, CA, USA, [2]University Grenoble Alpes, CNRS, IRD, Grenoble INP, IGE, Grenoble, France, [3]Centre for GeoGenetics, Natural History Museum of Denmark, University of Copenhagen, Copenhagen, Denmark, [4]NASA, Jet Propulsion Laboratory, Pasadena, CA, USA

Abstract We use a multisensor approach to assess the surge history over the past century of Storstrømmen and L. Bistrup Bræ, which drain the Northeast Ice Stream, Greenland. Storstrømmen surged around 1910 and Bistrup in 1913 and during the 1950s. Between 1978 and 1982, the speed of Storstrømmen peaked at 3 km/year during an active surge phase that lasted 10 years and the glacier has stayed in a quiescent phase since. Bistrup started to surge in 1988, peaked in 1993, and stopped in 1996. Both glaciers displayed a slow surge initiation and termination. Since 1993, ice builds up in the upper part of Storstrømmen at a 1 m/year, its lower part is thinning at its ablation rate of 1.4 m/year, and the grounding line has retreated by 10 km between 1992 and 2017, or 400 m/year. At these current rates, we project that Storstrømmen will meet presurge conditions in 2027–2030.

Plain Language Summary Storstrømmen and L. Bistrup Bræ in east Greenland probably are the largest surge-type glaciers in the world. Based on the history of frontal positions, it was suggested a surge periodicity on the order of 70 years. In this study, we use a multisensor approach combining historical data sets with the modern remote sensing techniques to reassess the surge history of Storstrømmen and document the unknown behavior of L. Bistrup Bræ. We found that, between 1978 and 1982, the speed of Storstrømmen peaked at more than 3 km/year during an active surge phase that lasted 10 years and the glacier has stayed in a quiescent phase since. L. Bistrup Bræ started to surge in 1988, peaked in 1993, and stopped in 1996. Since 1993, ice builds up in upper part of Storstrømmen at a 1 m/year, its lower part is thinning at its ablation rate of 1.4 m/year, and the grounding line has retreated by 10 km between 1992 and 2017. At these current rates of mass accumulation upstream and retreat downstream, we project that Storstrømmen will meet presurge conditions in 2027–2030.

1. Introduction

Glacier surge is a cyclic phenomenon, which is internally driven by oscillations in bed conditions that may lead to rapid episodic advances of the ice margin (Meier & Post, 1969; Sharp, 1988). Surge motion is caused by the rapid sliding induced by high water pressure (Robin & Weertman, 1973), which arises from a major restructuring of the basal hydraulic system from evolving glacier geometry and stress distribution (Kamb et al., 1985; Raymond, 1987). For marine terminating glaciers, a surge may cause the discharge of icebergs to the ocean to increase significantly, hence enhancing the rate of mass loss of the glacier. Changes in climate may affect the frequency of surges (Harrison & Post, 2003) or activate surging behavior (McMillan et al., 2014), which in turn impacts sea-level rise.

Storstrømmen and L. Bistrup Bræ are among the largest surge-type glaciers in the world (Higgins, 1991). Together with Zachariae Isstrøm and Nioghalvfjerdfjorden, they form the Northeast Greenland Ice Stream (M. A. Fahnestock et al., 2001; Figure 1a), which reaches far into the ice sheet to the flanks of Greenland's summit (Rignot & Mouginot, 2012). Storstrømmen and L. Bistrup Bræ flow, respectively, north and south around the nunatak complex of Dronning Louise Land, then merge again in Borgfjorden (Figure 1b). Their terminus positions have experienced large fluctuations over time: the glaciers retreated about 15 km between 1913 and 1950, remained stable from 1950 to 1978, and readvanced by 8 km between 1978 and 1984 (Reeh et al., 1994). This large frontal advance was recognized by Reeh et al. (1994) as a prolonged surge of Storstrømmen, which transferred 50 km^3 of ice from the upper basin to the lower part of the glacier (Figure 1b). Based on the history of frontal positions, the authors suggested a surge periodicity on the order of 70 years.

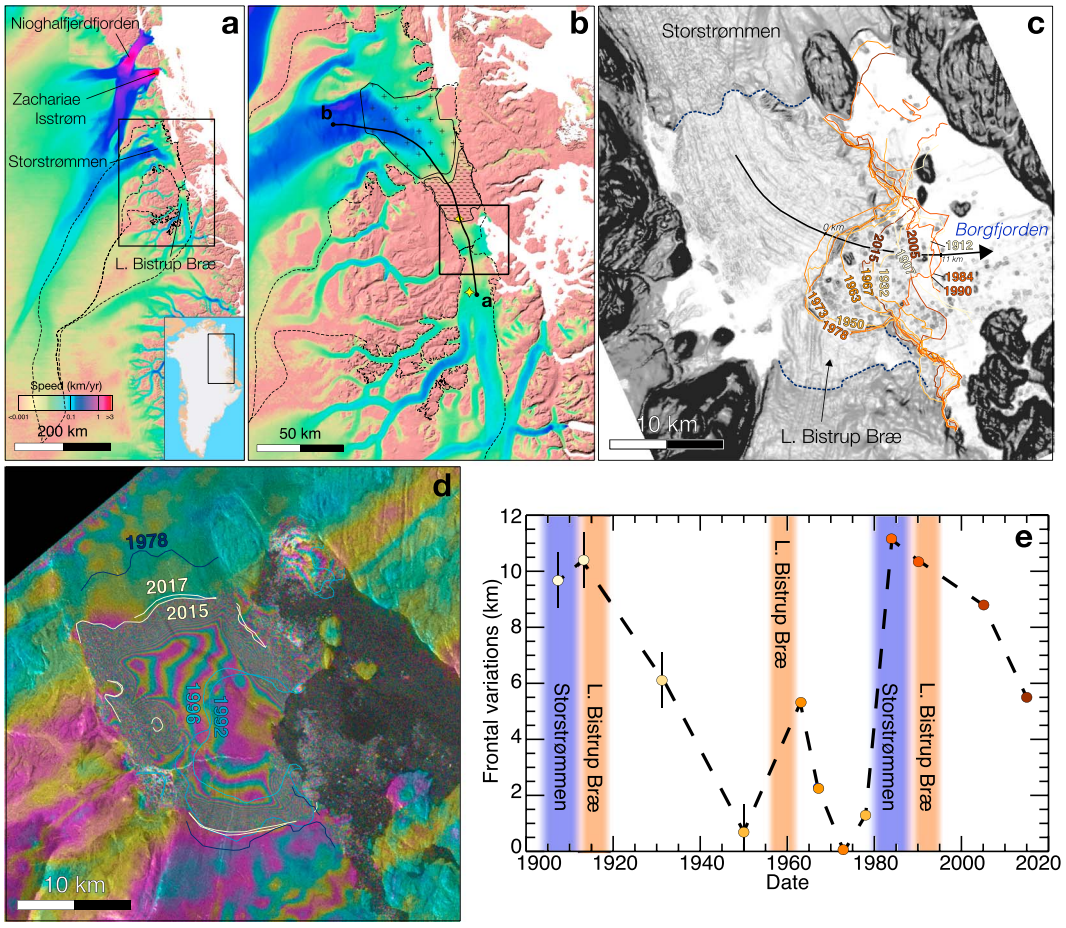

Figure 1. (a) Ice surface speed using a logarithmic scale of the northeast Greenland Ice Stream. Dotted lines are drainage basin boundaries of Storstrømmen and L. Bistrup Bræ. (b) Zoom of (a) on Storstrømmen and Bistrup. Black box indicates the location of (c) and (d). The regions annotated with (+) and (−) are the accumulation and ablation areas of Storstrømmen, respectively. Yellow stars indicate the regions of ice speed extraction in Figure 2. Segment a–b (black thick line) was flown by NASA in 1994, 1997, 2007, and 2014 (Figure 3). (c) Ice front location from 1907 (light orange) to 2017 (dark orange) overlaid on topographic slope from the 1978 DEM (Korsgaard et al., 2016) smoothed with a low-pass Gaussian filter of 200 m. Dashed black lines indicate a break in slope at the transition between grounded and floating ice. (d) Differential interferogram from Sentinel-1a/b showing the tidal-induced vertical motion in April 2017. (e) Ice front variations from 1907 to 2017 along the thick black arrow in (c). Frontal advances indicate surges of Storstrømmen (colored in purple) or L. Bistrup Bræ (colored in brown).

In this study, we use a multisensor approach combining historical data sets with the modern remote sensing techniques to (1) reassess the surge history of Storstrømmen between 1913 and 1990 as described by Reeh et al. (1994), (2) document the unknown behavior of L. Bistrup Bræ in response of the surge of Storstrømmen, (3) describe the evolution of the system since 1990, and (4) project when the next surge of Storstrømmen will occur.

2. Materials and Methods

We use historical maps, aerial, and satellite imagery to delineate the ice front positions of Storstrømmen and Bistrup Bræ over the last century. Although not accurate to modern standards, the historic maps are critical for providing historical information on the ice front positions in the earlier part of the 20th century. As shown in Figure 1c, the ice front position was first mapped during the 1906–1908 Denmark Expedition (Koch & Wegener, 1911, 1930; Reeh et al., 1994; Supporting Information Figure S1). In 1912, Koch and Wegener returned to northeast Greenland and made another detailed survey of the front (Koch & Wegener, 1930). The maps have been georeferenced near the ice margin using ground control points of recognizable

features. Aerial surveys were performed in 1932, 1950, 1963, 1967, 1968, and 1978 (Figures S2–S5). From 1973 to present, satellite images provide frequent coverage of the glaciers and their frontal positions with high precision. All aerial images are scanned at 600 dpi and georeferenced according to the 1978 orthorectified aerial photo (Korsgaard et al., 2016). For oblique aerial images (1932 and 1950) the procedure described in Bjørk et al. (2012) has been used, and only the areas encompassed by ground control points have been used to delineate the glacier margins (see Figures S2 and S3).

We build a 50-year time series of surface ice velocity using 10 satellite sensors and aerial platforms between 1967 and 2017. We estimate displacements between declassified CORONA images from August 1967 to March 1968 (Figure S6). Both images are orthorectified and precisely georeferenced before feature tracking using ice-free areas in the orthorectified 1978 aerial imagery (Korsgaard et al., 2016). We use Landsat-1&2/MSS images between 1973 and 1976 and combine image pairs up to 1 year apart to measure the displacement of surface features between images as described in Dehecq et al. (2015; two examples are given in Figures S7 and S8). We use the 1978 2-m orthorectified aerial images to correct the geolocation of Landsat-1 and -2 images (Korsgaard et al., 2016). Landsat did not acquire images over this glacier between 1976 and 1984, so we use alternate image sources. For 1978, we use an orthorectified American HEXAGON spy image acquired on 30 March that was declassified in 2013 (Figure S9), and orthorectified aerial pictures from Danish Survey acquired on 2 and 10 August (Figure S10). For 1982, we find another American HEXAGON spy image recently declassified. The image is resampled at 2-m spacing (original resolution between 60 cm and 1.2 m) and georeferenced to the 1978 aerial mosaic. Because the closest images in time from the spy data are the aerial photos from 1978 (4-year lapse) or Landsat-4 acquisitions from 1984 (2 years), feature tracking is impractical so we manually track in QGIS the migration of the meanders of supraglacial rivers at the center of Storstrømmen (Figure S11). The 1982 HEXAGON image is not orthorectified, but we estimate that the induced errors on the relatively flat glacier surface are negligible compared to the large glacier displacement observed between the periods 1978–1982 (12 km) and 1982–1984 (3.2 km). Between 1984 and 1991, 684 Landsat-4&5/TM image pairs were acquired up to 1-year apart (Figure S12). Only a few Landsat-4 and -5 images (~3%) needed geocoding refinement using the 1978 reference as used previously. Between 1991 and 1998, we process radar images from the European ERS-1/2, with a repeat cycle varying from 3 to 36 days depending on the mission phase (Figure S13). Between 1999 and 2013, we use RADARSAT-1/2, ALOS/PALSAR, ENVISAT/ASAR to determine surface velocity (Joughin et al., 2010; Rignot & Mouginot, 2012). After 2013, we use Landsat-8, Sentinel-1a/b, and RADARSAT-2 (Mouginot et al., 2017). All synthetic aperture radar (SAR) data sets are processed assuming surface parallel flow using the digital elevation model (DEM) from the Greenland Mapping Project (Howat et al., 2014) and calibrated as described in Mouginot et al. (2012, 2017).

We map the glacier grounding line using InSAR data from the European Earth Remote Sensing (ERS-1/2) radar satellite collected in 1992 (3-day repeat cycle), in 1996 (1-day apart), and Sentinel-1a/b in November 2015 and April 2017 (Scheuchl et al., 2016). We employ differential InSAR technique (Rignot et al., 2011) on interferograms from radar images within the same month. After correcting the signal for surface topography using 2014 Greenland Mapping Project DEM, we use the differential interferograms to quantify the short-term vertical motion of the ice forced by changes in oceanic tides (Figure 1d). To digitize the grounding lines, we pick the inward limit of detection of vertical motion, where the glacier becomes afloat with a precision of about 50 m, as in Rignot et al. (2011). In addition to the InSAR grounding lines, we estimate the grounding position from the 1978 DEM using the break in slope (Figure 1c) with a precision of about 500 m (Rignot et al., 2011).

Finally, we document the evolution of the ice surface elevation and ice thickness along a flight track from NASA's Operation IceBridge over Storstrømmen and L. Bistrup Bræ (Figure 3). As provided by the Center for Remote Sensing of Ice Sheets, ice thickness is calculated assuming a real dielectric constant of 3.15 for ice with no firn correction and associated error of about 25 m. We use the 25-m posting 1978 topography derived from aerial imagery (Korsgaard et al., 2016), the scanning LiDAR Airborne Topographic Mapper operated by NASA between 1993 and 2014 (Brunt et al., 2017), the Multichannel Coherent Radar Depth Sounder operated by Center for Remote Sensing of Ice Sheets through NASA programs between 1999 and 2014 (Gogineni et al., 1998; Rodriguez-Morales et al., 2014), and the time-dependent ArticDEMs created by the Polar Geospatial Center from DigitalGlobe, Inc. imagery.

3. Results

Figures 1c and 1e show the ice front evolution along their center flowline of Storstrømmen (indicated by the black arrow in Figure 1c) since 1907. During the Denmark expedition of 1907–1908 (Figure S1), the terminus was at an advanced position and continued to advance until the next expedition in 1912–1913 (Figure S2). In April 1913, Koch and Wegener (1930) witnessed a change in the flow of L. Bistrup Bræ near their camp site and described it as a speedup. This speedup may have been part of a surge and fits well with the assumed periodicity of L. Bistrup Bræ surges. Aerial pictures taken in 1932 (Figure S3) suggest that the ice margins retreated by about 5 km by 1932 and another 5–6 km by 1950 (Figure S4), hence reaching the most retreated known position of the glacier in the past century. Other aerial images taken in 1963 indicate that the front advanced about 5 km compared to 1950, but retreated again by roughly 3 km in 1966 and another 2 km by 1973 to reach its most retreated state, which is not documented in Reeh et al. (1994). Between 1973 and 1984, the front position advanced rapidly by 12 km to reach a similar position as during the 1913 stage. Since 1984, the front has retreated by about 5 km, approximately halfway between the known extremes for advance and retreat of the front. The similarity between the 1913 and 1984 frontal positions suggests that the 1913 advance of the glacier front was the result of a rapid advance due to the surge of Storstrømmen. Reeh et al. (1994), however, did not report the front advance between 1950 and 1963. Although the 1950s image is oblique and so distorted when georeferenced, the comparison with the aerial image taken in 1963 shows that the supraglacial medial moraine in the center of L. Bistrup Bræ moved forward, its ice front advanced by 5–6 km, and the suture zone between Bistrup and Storstrømmen migrated northward, that is, toward Storstrømmen (see Figures S4–S7). This suggests that the 5-km advance of the terminus observed between 1950 and 1963 should be attributed to a surge of L. Bistrup Bræ and that the active surging phase centered around 1963.

Figure 1d shows the grounding position in 1978, 1992, 1996, 2015, and 2017. The 1978 position is the most upstream known position of the grounding line. Between 1978 and 1992, the grounding line of Storstrømmen and L. Bistrup Bræ advanced by 14 and 1.5 km, respectively. While Storstrømmen's grounding line remained relatively stable between 1992 and 1996, the grounding line of L. Bistrup Bræ's advanced by 3.5 km over the same time period. Since then, both grounding lines have retreated significantly. L. Bistrup Bræ is back to its 1992 position and Storstrømmen has retreated 10 km since 1992, or 400 m/year, and is now 5 km downstream of its 1978 position.

Figure 2 shows the ice velocity evolution from 1967 to present. Storstrømmen was flowing at a slow pace (about 0.2 km/year) between 1967 and 1976. Its speed increased to reach an averaged maximum speed of 3 km/year between 1978 and 1982. After 1982, Storstrømmen speed steadily decreased to a near stop by 1991. Since then, the glacier has returned to background velocity rates.

The behavior of L. Bistrup Bræ follows a similar pattern as Storstrømmen but shifted by 10 years. Its speed was relatively low, around 0.1 km/year, between 1974 and 1986. After 1986, the speed of L. Bistrup Bræ started to increase, first slowly to reach 0.45 km/year in 1990, then abruptly to 1.35 km/year by 1993. Between 1993 and 1996, a sharp decrease in speed is observed back to its previous slow state. Since then, the glacier has displayed only small seasonal changes in speed ($<$0.1 km/year; Figure 2b).

Figure 3 shows the change in surface elevation along the NASA's Airborne Topographic Mapper flight line between 1993 and 2014, the ArcticDEMs between 2012 and 2015, and the Multichannel Coherent Radar Depth Sounder radar sounder in 1999 and 2014 (Figure 1b). The upper part of Storstrømmen has thickened at a rate of 1.0 m/year since 1993 (63 km above the 1978 grounding line), while the lower part has thinned at 1.4 m/year (7 km above the 1978 grounding line). The transition between thinning (lower) and thickening (upper) regions of Storstrømmen is about 20–22 km above the 1978 grounding line.

4. Discussion

The last surge of Storstrømmen in 1982 reported by Reeh et al. (1994) did not include satellite or aerial images between 1978 and 1989, hence could not resolve the entire surge cycle. Here we find that the active surge phase lasted 10 years, or twice as long as reported by Reeh et al. (1994). Since 1988, Storstrømmen has been in a quiescent phase, with ice building up in a reservoir area in the upper part (115 to 80 km in Figures 3a and 3b) of the glacier, while its lower part (70 to 115 km in Figures 3a and 3b), near the terminus, is thinning.

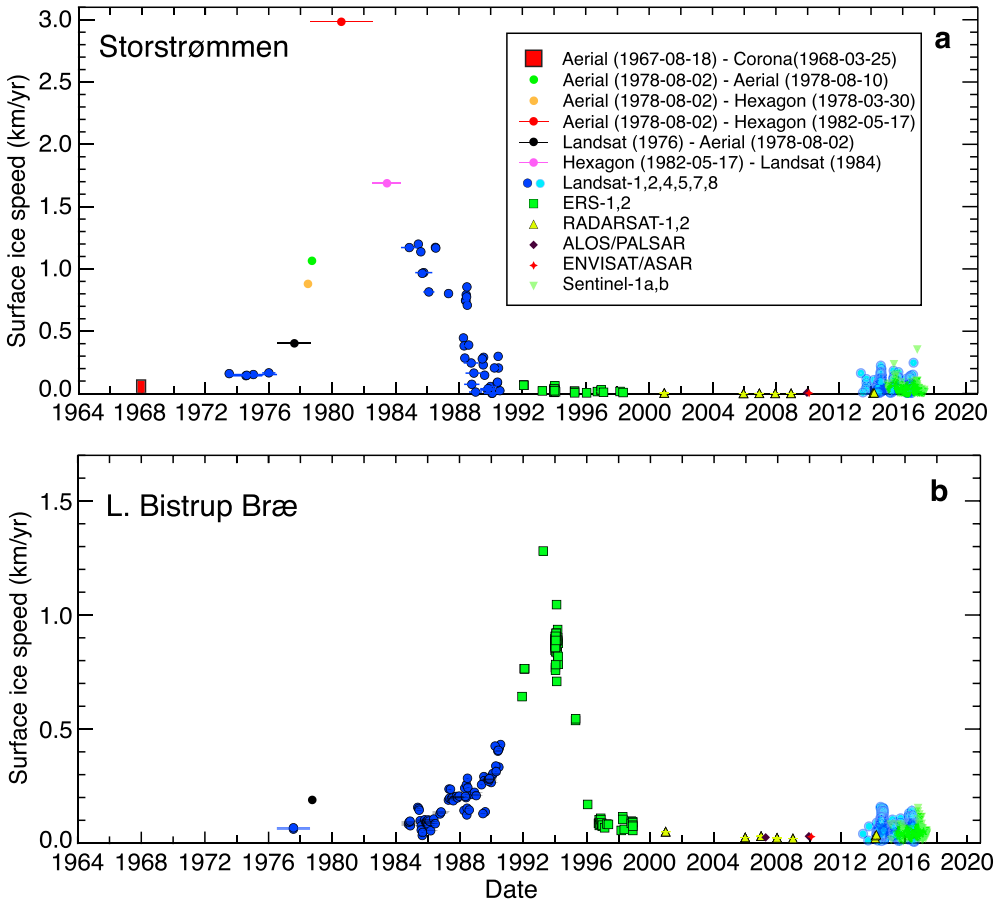

Figure 2. Time series of ice speed from 1964 to 2017 of (a) Storstrømmen and (b) L. Bistrup Bræ with sensor defined by color and symbol, at locations defined by yellow stars in Figure 1b.

We document for the first time the surge behavior of L. Bistrup Bræ which started in 1988, when the surge of Storstrømmen ended. This cycling is consistent with the observations by Koch and Wegener between 1907 and 1913. Yet it is not clear how the surges of the two glaciers are coupled. On the one hand, the two glaciers coalesce at their common ice front and therefore may exert back forces to one another. On the other hand, the ice front history suggests that the surge of L. Bistrup Bræ in the 1950s did not follow the surge of Storstrømmen. Our reconstruction suggests that the surge cycle for the two glaciers is 70 years for Storstrømmen (~1910 and 1982) versus 30–50 years for L. Bistrup Bræ (~1912, the 1950s, 1993; Figure 1e), which means that the surge cycles are different. Since 1997, L. Bistrup Bræ is also in a quiescent phase, with ice thickening in the upper part (10 to 40 km) while its lower part is thinning (40 to 70 km in Figures 3a and 3b).

From the combination of ice thickness and ice velocity reported here, we estimate that the total ice discharge during the surges of Storstrømmen (1975–1988) and L. Bistrup Bræ (1985–1996) is 126+/−14 and 11+/−2 Gt, respectively. Reeh et al. (1994) estimated that 50 km^3 (45 Gt between 1978 and 1984) was transferred for the upper to the lower part of Storstrømmen, or half our estimate. Using the output of the regional climate model RACMOv2.3p2 downscaled at 1 km (Noël et al., 2018), we find that the average surface mass balance for the period 1960–1989 for Storstrømmen and L. Bistrup Bræ was 1.7+/−0.8 and 1.0+/−0.3 Gt per year, respectively. Using this average SMB value, the total mass accumulated over Storstrømmen basin between two surges (1910 and 1982) should be 121 and 37 Gt for L. Bistrup Bræ between the surges of the 1950s and 1993. The 126 Gt discharged by Storstrømmen during its last surge is therefore comparable with the accumulated ice mass during 72 years, which means that the surge brought the glacier to a state of mass balance over a period of 70 years. In contrast, the 11 Gt discharge by L. Bistrup Bræ during the 1993 surge is 3 times smaller than the mass accumulated over its basin based on RACMO. Several reasons could explain the

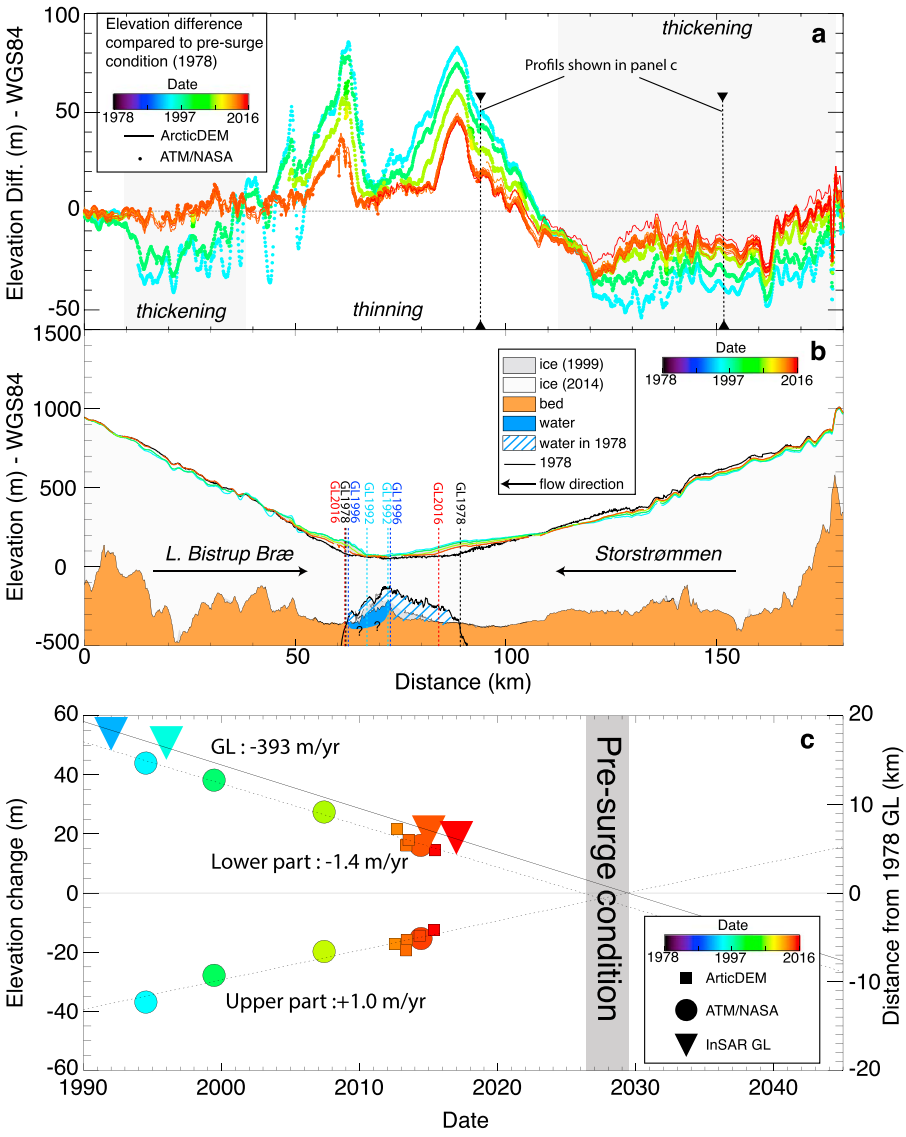

Figure 3. Change in surface elevation of Storstrømmen and L. Bistrup Bræ (a) measured with ATM/NASA data, ArcticDEM data compared to the 1978 DEM and (b) bed elevation from the MCoRDS radar sounder along profile in Figure 1b (thick black line). Black line near bed indicates the ice bottom elevation derived from floatation using the 1978 DEM (ice density = 917 kg/m^3 and sea water = 1,024 kg/m^3). Hatched blue is ocean water in 1978. (c) Time series of elevation change of the upper and lower parts of Storstrømmen measured with ATM/NASA (circles) and ArcticDEM (squares) compared to the 1978 DEM at the locations indicated by black vertical dashed lines in (a), and time series of distance from 1978 grounding line (triangles) along the black arrow profile in Figure 1a. The 1978 state of Storstrømmen represents surge initiation (gray box). Each time series is linearly extrapolated (dashed and solid black lines) to intercept in 2027–2030 when the 1978 conditions will be repeated. DEM = digital elevation model; ATM = Airborne Topographic Mapper.

difference for L. Bistrup Bræ. One possibility is that the mass discharge by L. Bistrup Bræ varies from one surge to the next and that the last surge was small, for example, because the recent surge of Storstrømmen had already transferred a large amount of ice to the lower part, hence obstructing the flow of L. Bistrup Bræ through Borgfjorden. Another possibility is that L. Bistrup may have surged in the 1930s, for which we have no data, that is, its surge cycle is closer to 30 years or may also be irregular.

Since the end of the surges in 1988 (Storstrømmen) and 1996 (L. Bistrup Bræ), we observe that the glaciers are returning to their presurge configurations. Storstrømmen's upper part is thickening at 1 m/year (Figure 3c), while its lower part is thinning at a rate of 1.4 m/year, similar to the average thinning modeled by RACMO (1.3+/−0.1 m/year between 1992 and 2017), that is, the glacier lower reaches are thinning at their ablation

rate. The grounding lines and ice fronts are retreating, thus reducing basal friction and back pressure applied on the upper parts, similar to the mechanism that lead to the destabilization of a glacier in Svalbard described by McMillan et al. (2014). The 1978 DEM and grounding line position reveal the glacier configuration at the inception of Storstrømmen surge. It is reasonable to expect that if the same conditions are reproduced in years to come, the system will surge again. The surge will repeat if the boundary conditions are repeated and the amount of mass that accumulates upstream reaches a similar level. While we do not know the surging configuration of L. Bistrup Bræ in 1988 that would allow us to extrapolate its next surge, we have information from the 1978 DEM at the onset of Storstrømmen's surge.

Between 1994 and 2014, the upstream surface elevation of Storstrømmen from 20 to 60 km above the 1978 grounding line has increased up to 20 m while the downstream elevation (0 to 20 km above the 1978 grounding line) decreased by up to 30 m (Figure 3a). If we assume that the 1978 conditions correspond to a presurge state, with similar rates of thinning, thickening, and grounding line retreat to those observed between 1992 and 2017, we estimate that the presurge configuration will be met between 2027 and 2030 (Figure 3c). If correct, the surge period of Storstrømmen will be 52 years instead of 72 years from Reeh et al. (1994) and ice front reconstruction. The 28% shorter cycle may be linked to a change in recent climate. Indeed, the surface ablation rate of the lower part of the glacier modeled by RACMO has increased by 25% between the periods 1958–1970 and 2010–2017. While the change in subaqueous melting of the glacier floating sections is not known, several studies suggests that ocean temperature is warming around Greenland (Rignot et al., 2012; Straneo et al., 2010), which would lead to faster retreat of the grounding line.

Surge motion is usually caused by rapid basal sliding due to high water pressure (Robin & Weertman, 1973), which arises from a restructuring of the basal hydraulic system from an evolving glacier geometry and stress distribution (Kamb et al., 1985; Raymond, 1987). The initiation of the surges of Storstrømmen or L. Bistrup Bræ took years to buildup. The velocity map from 1973 to 1975 (see Supplemental Materials), 8 years before the peak active phase, shows that Storstrømmen was already flowing at a slow pace of 150 to 200 m/year. The initiation and termination of the surges observed here differ from those in Alaska (e.g., Variaegated, Bering, or West Fork glaciers) or Sortebræ, east Greenland (Pritchard et al., 2003, 2005), that started and ended suddenly with the same seasonal timing: winter–summer. Storstrømmen and Bistrup surges are more characteristic of surging glaciers found in Svalbard (Murray et al., 2002) or the Canadian Artic (Millan et al., 2017; Van Wychen et al., 2016) with slow initiation or termination and long active phases. The Svalbard style of surge (slow initiation and termination) has been explained by a switch between frozen and unfrozen bed conditions (Clarke, 1976; Fowler et al., 2001), which leads to meltwater production and therefore a rise in basal pressure. The buildup of ice mass increases the driving stress, which generates more heat. For Storstrømmen, it would be necessary to evaluate if the relatively small change in thickness (+2%) during the quiescent period is sufficient to generate enough heat to raise the bed to the pressure melting point.

The denser velocity measurements gathered between 1988 and 1990 reveal that, toward the end of the active phase, Storstrømmen displayed strong seasonal fluctuations with maximum speed in July and slower speeds in winter (Figure 2a). This observation suggests that the glacier flow was probably controlled by the seasonal input of subglacial water. This could in turn imply that meltwater was able to accumulate at the base of the glacier and raise basal pressure (Kamb, 1987). Although production of surface melt water is limited in the accumulation area and above, Storstrømmen and L. Bistrup are part of Northeast Greenland Ice Stream which experiences significant ice melt at the base as shown by ice penetrating radar and ice core drilling (M. A. Fahnestock et al., 2001; Grinsted & Dahl-Jensen, 2002; Oswald & Gogineni, 2012) due to anomalously high geothermal flux (Rogozhina et al., 2016) and enhanced basal friction (M. Fahnestock et al., 2001). Some of this meltwater is likely routed toward Storstrømmen and L. Bistrup Bræ, where it would accumulate. As shown in Figure 3b, about 130 km upstream the grounding line, Storstrømmen's bedrock drops by 1,000 from 600 m above sea level to 400 m below sea level, and then rises again to 100 m below sea level about 100 km from the grounding line. A similar configuration is observed on the accumulation area of L. Bistrup Bræ where the bedrock altitude decreases from 150 m above sea level to 500 m below sea level and then rise to 100 m below sea level (Figure 3b). These deep basins form natural reservoirs for subglacial water to accumulate.

The *slow* surge probably initiates when a combination of high basal water pressure or total accumulation of mass (water or ice), and reduced back pressure from the lower part or retreat of the grounding line past the

1978 limit, is reached. The surge terminates when enough mass has been transferred from the upper to the lower parts, hence offering renewed back pressure to the upper system. A participant to the grounding line retreat may be the subaqueous melting of the glacier floating section (Figure 3b). At Zachariae Isstrøm, an increase in ocean temperature combined with a decrease in ice mélange gluing the ice shelf bits together were likely the main drivers for more rapid iceberg detachment and glacier acceleration (Khan et al., 2014; Mouginot et al., 2015). The ocean conditions and bathymetry at the front of Storstrømmen and L. Bistrup Bræ are unknown at present, but are of interest to refine our understanding of the conditions that lead to surge conditions, in particular to define the role of ocean thermal forcing in constraining the retreat of the ice front, if any.

5. Conclusions

Using a multisensor approach, we assess the surge history between 1907 and 2017 of Storstrømmen and L. Bistrup Bræ. Both glaciers have been in a quiescent phase since 1988/1996 but we project that conditions leading to a surge, including total thickening in the upstream area and grounding line retreat in the lower reaches, will likely be repeated around 2027 and 2030 for Storstrømmen. The study demonstrates the practical use of historical data spanning nearly one century, reanalyzed with modern constraints, to understand the long-term history of northeast Greenland surging glaciers.

Acknowledgments

This work was performed under a grant with the National Aeronautics and Space Administration's Cryosphere Program. We acknowledge the European Union Copernicus Program, ESA, CSA, JAXA, ASI, and DLR for the use of SAR data, NASA and USGS for the Landsat-8, and NASA's OIB mission. We thank STG and PSTG for coordinating satellite data acquisition efforts during IPY and post IPY, respectively. A.A.B. was supported by the Independent Research Fund Denmark (grant DFF-610800469) and by the Inge Lehmann Scholarship from the Royal Danish Academy of Science and Letters. We are grateful for the support from the former National Danish Survey and Cadastre, now Department of Data-supply and Efficiency, for access to historical aerial imagery. Ice speed, grounding line, and ice front data sets used in this article can be obtained from https://doi.pangaea.de/10.1594/PANGAEA.894762. The 1978 DEM is available from NOAA National Centers for Environmental Information (https://doi.org/10.7289/V56Q1V72); the ATM data were distributed by NSIDC (https://nsidc.org/data/ILATM2); the ice thickness data are available from CReSIS (https://data.cresis.ku.edu/); ArcticDEM are distributed by the Polar Geospatial Center (https://www.pgc.umn.edu/data/arcticdem/); Landsat, Corona, and Hexagon images are freely distributed by USGS (https://earthexplorer.usgs.gov/); ERS and Sentinel images are freely distributed by ESA (https://scihub.copernicus.eu); other speed data are available from NASA MEaSUREs data sets from NSIDC (https://nsidc.org/data/measures/data_summaries). Thanks to the two reviewers for their constructive comments and helpful suggestions on an earlier version of the manuscript.

References

Bjørk, A. A., Kjær, K. H., Korsgaard, N. J., Khan, S. A., Kjeldsen, K. K., Andresen, C. S., et al. (2012). An aerial view of 80 years of climate-related glacier fluctuations in southeast Greenland. *Nature Geoscience*, *5*, 427–432. https://doi.org/10.1038/ngeo1481

Brunt, K. M., Hawley, R. L., Lutz, E. R., Studinger, M., Sonntag, J. G., Hofton, M. A., et al. (2017). Assessment of NASA airborne laser altimetry data using ground-based GPS data near Summit Station, Greenland. *The Cryosphere*, *11*(2), 681–692. https://doi.org/10.5194/tc-11-681-2017

Clarke, G. K. C. (1976). Thermal regulation of glacier surging. *Journal of Glaciology*, *16*(74), 231–250. https://doi.org/10.1017/S0022143000031567

Dehecq, A., Gourmelen, N., & Trouve, E. (2015). Deriving large-scale glacier velocities from a complete satellite archive: Application to the Pamir-Karakoram-Himalaya. *Remote Sensing of Environment*, *162*, 55–66. https://doi.org/10.1016/j.rse.2015.01.031

Fahnestock, M., Abdalati, W., Joughin, I., Brozena, J., & Gogineni, P. (2001). High geothermal heat flow, basal melt, and the origin of rapid ice flow in central Greenland. *Science*, *294*(5550), 2338–2342. https://doi.org/10.1126/science.1065370

Fahnestock, M. A., Joughin, I., Scambos, T. A., Kwok, R., Krabill, W. B., & Gogineni, S. (2001). Ice-stream-related patterns of ice flow in the interior of northeast Greenland. *Journal of Geophysical Research*, *106*(D24), 34,035–34,045. https://doi.org/10.1029/2001JD900194

Fowler, A. C., Murray, T., & Ng, F. S. L. (2001). Thermally controlled glacier surging. *Journal of Glaciology*, *47*(159), 527–538. https://doi.org/10.3189/172756501781831792

Gogineni, S., Chuah, T., Allen, G., Jezek, K., & Moore, R. K. (1998). An improved coherent radar depth sounder. *Journal of Glaciology*, *44*(148), 659–669. https://doi.org/10.1017/S0022143000002161

Grinsted, A., & Dahl-Jensen, D. (2002). A Monte Carlo-tuned model of the flow in the NorthGRIP area. *Annals of Glaciology*, *35*, 527–530. https://doi.org/10.3189/172756402781817130

Harrison, W. D., & Post, A. S. (2003). How much do we really know about glacier surging? *Annals of Glaciology*, *36*, 1–6. https://doi.org/10.3189/172756403781816185

Higgins, A. K. (1991). North Greenland glacier velocities and calf ice production. *Polarforschung, Bremerhaven, Alfred Wegener Institute for Polar and Marine Research & German Society of Polar Research*, *60*(1), 1–23.

Howat, I. M., Negrete, A., & Smith, B. E. (2014). The Greenland Ice Mapping Project (GIMP) land classification and surface elevation data sets. *The Cryosphere*, *8*(4), 1509–1518. https://doi.org/10.5194/tc-8-1509-2014

Joughin, I., Smith, B. E., & Abdalati, W. (2010). Glaciological advances made with interferometric synthetic aperture radar. *Journal of Glaciology*, *56*(200), 1026–1042. https://doi.org/10.3189/002214311796406158

Kamb, B. (1987). Glacier surge mechanism based on linked cavity configuration of the basal water conduit system. *Journal of Geophysical Research*, *92*(B9), 9083. https://doi.org/10.1029/JB092iB09p09083

Kamb, B., Raymond, C. F., Harrison, W. D., Engelhardt, H., Echelmeyer, K. A., Humphrey, N., et al. (1985). Glacier surge mechanism: 1982-1983 surge of Variegated Glacier, Alaska. *Science*, *227*(4686), 469–479. https://doi.org/10.1126/science.227.4686.469

Khan, S. A., Kjær, K. H., Bevis, M., Bamber, J. L., Wahr, J., Kjeldsen, K. K., et al. (2014). Sustained mass loss of the northeast Greenland ice sheet triggered by regional warming. *Nature Climate Change*, *4*(4), 292–299. https://doi.org/10.1038/nclimate2161

Koch, J. P., & Wegener, A. (1911). Die glaziologischen Beobachtungen der Danmark-expedition. *Meddr Grønland*, *46*(1), 77.

Koch, J. P., & Wegener, A. (1930). Wissenschaftliche Ergebnisse der dänischen Expedition nach Dronning Louises Land und quer über das Inlandeis von Nordgrönland 1912-1913 unter Leitung von Hauptmann J. P. Koch. *Meddr Grønland*, *75*(1), 676.

Korsgaard, N. J., Nuth, C., Khan, S. A., Kjeldsen, K. K., Bjørk, A. A., Schomacker, A., et al. (2016). Digital elevation model and orthophotographs of Greenland based on aerial photographs from 1978-1987. *Scientific Data*, *3*, 160032. https://doi.org/10.1038/sdata.2016.32

McMillan, M., Shepherd, A., Gourmelen, N., Dehecq, A., Leeson, A., Ridout, A., et al. (2014). Rapid dynamic activation of a marine-based Arctic ice cap. *Geophysical Research Letters*, *41*, 8902–8909. https://doi.org/10.1002/2014GL062255

Meier, M. F., & Post, A. (1969). What are glacier surges? *Canadian Journal of Earth Sciences*, *6*(4), 807–817. https://doi.org/10.1139/e69-081

Millan, R., Mouginot, J., & Rignot, E. (2017). Mass budget of the glaciers and ice caps of the Queen Elizabeth Islands, Canada, from 1991 to 2015. *Environmental Research Letters*, *12*(2). https://doi.org/10.1088/1748-9326/aa5b04

Mouginot, J., Rignot, E., Scheuchl, B., Fenty, I., Khazendar, A., Morlighem, M., et al. (2015). Fast retreat of Zachariæ Isstrøm, northeast Greenland. *Science*, *350*(6266), 1357–1361. https://doi.org/10.1126/science.aac7111

Mouginot, J., Rignot, E., Scheuchl, B., & Millan, R. (2017). Comprehensive annual ice sheet velocity mapping using Landsat-8, Sentinel-1, and RADARSAT-2 data. *Remote Sensing*, *9*(4). https://doi.org/10.3390/rs9040364

Mouginot, J., Scheuch, B., & Rignot, E. (2012). Mapping of ice motion in Antarctica using synthetic-aperture radar data. *Remote Sensing*, *4*(9), 2753–2767. https://doi.org/10.3390/rs4092753

Murray, T., Strozzi, T., Luckman, A., Pritchard, H., & Jiskoot, H. (2002). Ice dynamics during a surge of Sortebræ, east Greenland. *Annals of Glaciology*, *34*, 323–329. https://doi.org/10.3189/172756402781817491

Noël, B., van de Berg, W. J., van Wessem, J. M., van Meijgaard, E., van As, D., Lenaerts, J. T. M., et al. (2018). Modelling the climate and surface mass balance of polar ice sheets using RACMO2 – Part 1: Greenland (1958–2016). *The Cryosphere*, *12*, 811–831. https://doi.org/10.5194/tc-12-811-2018

Oswald, G. K. A., & Gogineni, S. P. (2012). Mapping basal melt under the northern Greenland ice sheet. *IEEE Transactions on Geoscience and Remote Sensing*, *50*(2), 585–592. https://doi.org/10.1109/TGRS.2011.2162072

Pritchard, H., Murray, T., Luckman, A., Strozzi, T., & Barr, S. (2005). Glacier surge dynamics of Sortebrae, east Greenland, from synthetic aperture radar feature tracking. *Journal of Geophysical Research*, *110*, F03005. https://doi.org/10.1029/2004JF000233

Pritchard, H., Murray, T., Strozzi, T., Barr, S., & Luckman, A. (2003). Surge-related topographic change of the glacier Sortebrae, east Greenland, derived from synthetic aperture radar interferometry. *Journal of Glaciology*, *49*(166), 381–390. https://doi.org/10.3189/172756503781830593

Raymond, C. F. (1987). How do glaciers surge? A review. *Journal of Geophysical Research*, *92*(B9), 9121. https://doi.org/10.1029/JB092iB09p09121

Reeh, N., Boggild, C. E., & Oerter, H. (1994). Surge of Storstrømmen, a large outlet glacier from the inland ice of north-east Greenland. *Grønlands Geologiske Undersøgelses, Rapp*, *162*, 201–209.

Rignot, E., Fenty, I., Menemenlis, D., & Xu, Y. (2012). Spreading of warm ocean waters around Greenland as a possible cause for glacier acceleration. *Annals of Glaciology*, *53*(60), 257–266. https://doi.org/10.3189/2012AoG60A136

Rignot, E., & Mouginot, J. (2012). Ice flow in Greenland for the international polar year 2008-2009. *Geophysical Research Letters*, *39*, L11501. https://doi.org/10.1029/2012GL051634

Rignot, E., Mouginot, J., & Scheuchl, B. (2011). Antarctic grounding line mapping from differential satellite radar interferometry. *Geophysical Research Letters*, *38*, L10504. https://doi.org/10.1029/2011GL047109

Robin, G. D. Q., & Weertman, J. (1973). Cyclic surging of glaciers. *Journal of Glaciology*, *12*(64), 3–18. https://doi.org/10.1017/S002214300002267X

Rodriguez-Morales, F., Gogineni, S., Leuschen, C. J., Paden, J. D., Li, J., Lewis, C. C., et al. (2014). Advanced multifrequency radar instrumentation for polar research. *IEEE Transactions on Geoscience and Remote Sensing*, *52*(5), 2824–2842. https://doi.org/10.1109/TGRS.2013.2266415

Rogozhina, I., Petrunin, A. G., Vaughan, A. P. M., Steinberger, B., Johnson, J. V., Kaban, M. K., et al. (2016). Melting at the base of the Greenland ice sheet explained by Iceland hotspot history. *Nature Geoscience*, *9*(5), 366–369. https://doi.org/10.1038/ngeo2689

Scheuchl, B., Mouginot, J., Rignot, E., Morlighem, M., & Khazendar, A. (2016). Grounding line retreat of Pope, Smith, and Kohler Glaciers, West Antarctica, measured with Sentinel-1a radar interferometry data. *Geophysical Research Letters*, *43*, 8572–8579. https://doi.org/10.1002/2016GL069287

Sharp, M. (1988). Surging glaciers: Behaviour and mechanisms. *Progress in Physical Geography*, *12*(3), 349–370. https://doi.org/10.1177/030913338801200302

Straneo, F., Hamilton, G. S., Sutherland, D. A., Stearns, L. A., Davidson, F., Hammill, M. O., et al. (2010). Rapid circulation of warm subtropical waters in a major glacial fjord in east Greenland. *Nature Geoscience*, *3*(3), 182–186. https://doi.org/10.1038/ngeo764

Van Wychen, W., Davis, J., Burgess, D. O., Copland, L., Gray, L., Sharp, M., et al. (2016). Characterizing interannual variability of glacier dynamics and dynamic discharge (1999-2015) for the ice masses of Ellesmere and Axel Heiberg Islands, Nunavut, Canada. *Journal of Geophysical Research: Earth Surface*, *121*, 39–63. https://doi.org/10.1002/2015JF003708